



## Article

# Enhanced Solar Efficiency via Incorporation of Plasmonic Gold Nanostructures in a Titanium Oxide/Eosin Y Dye-Sensitized Solar Cell

Sanele Nyembe <sup>1,\*</sup>, Francis Chindeka <sup>2</sup>, Gebhu Ndlovu <sup>3</sup>, Andile Mkhohlakali <sup>1</sup>, Tebello Nyokong <sup>2</sup> and Lucky Sikhwivhilu <sup>3,4</sup>

- <sup>1</sup> Analytical Chemistry Division/Mintek, Private Bag X3015, Randburg, Johannesburg 2125, South Africa; andilem@mintek.co.za
- <sup>2</sup> Institute for Nanotechnology Innovation, Department of Chemistry, Rhodes University, Grahamstown 6140, South Africa; f.chindeka@ru.ac.za (F.C.); t.nyokong@ru.ac.za (T.N.)
- <sup>3</sup> DST/Mintek Nanotechnology Innovation Centre, Mintek, Private Bag X3015, Randburg, Johannesburg 2125, South Africa; gebhun@mintek.co.za (G.N.); luckys@mintek.co.za (L.S.)
- <sup>4</sup> Department of Chemistry, Faculty of Science, Engineering and Agriculture, University of Venda, Private Bag X5050, Thohoyandou 0950, South Africa
- \* Correspondence: saneleny@mintek.co.za; Tel.: +27-11-709-4768

**Abstract:** Plasmonic gold nanoparticles significantly improved the efficiency of a TiO<sub>2</sub> and Eosin Y based dye-sensitized solar cell from 2.4 to 6.43%. The gold nanoparticles' sizes that were tested were 14 nm, 30 nm and 40 nm synthesized via the systematic reduction of citrate concentration using the Turkevich method. Pristine TiO<sub>2</sub> without plasmonic gold nanoparticles yielded an efficiency of 2.4%. However, the loading of 40 nm gold nanoparticles into the TiO<sub>2</sub> matrix yielded the highest DSSC efficiency of 6.43% compared to 30 nm (5.91%) and 14 nm (2.6%). The relatively high efficiency demonstrated by plasmonic gold nanoparticles is ascribed to light absorption/scattering, hot electron injection and plasmon-induced resonance energy transfer (PIRET), influenced by the size of the gold nanoparticles.

**Keywords:** gold nanoparticles; titanium oxide; dye-sensitized solar cell; photon-to-electron conversion efficiency; hot electron injection mechanism; charge recombination



**Citation:** Nyembe, S.; Chindeka, F.; Ndlovu, G.; Mkhohlakali, A.; Nyokong, T.; Sikhwivhilu, L. Enhanced Solar Efficiency via Incorporation of Plasmonic Gold Nanostructures in a Titanium Oxide/Eosin Y Dye-Sensitized Solar Cell. *Nanomaterials* **2022**, *12*, 1715. <https://doi.org/10.3390/nano12101715>

Academic Editors: Farida Selim, Yongqiang Wang and Baizeng Fang

Received: 6 April 2022

Accepted: 13 May 2022

Published: 17 May 2022

**Publisher's Note:** MDPI stays neutral with regard to jurisdictional claims in published maps and institutional affiliations.



**Copyright:** © 2022 by the authors. Licensee MDPI, Basel, Switzerland. This article is an open access article distributed under the terms and conditions of the Creative Commons Attribution (CC BY) license (<https://creativecommons.org/licenses/by/4.0/>).

## 1. Introduction

Global electrical energy consumption is currently at an overwhelming 16 terawatt (TW), which includes transportation, agriculture, industry, heating, etc. [1,2]. The current global population increase rate of 1.1% per year and the adaption of the modern way of life due to urbanization will catapult the global energy consumption to 29 TW in less than 15 years [3,4]. The majority of the 16 TW energy consumption (12 TW) is from burning fossil fuels [3]. Hence, there is a growing requirement for global renewable energy sources in order to eradicate the dependency on finite fossil fuels. Dye-sensitized solar cells (DSSCs) are a promising renewable energy source owing to the low production cost and relatively high photo-to-electron conversion efficiency [5,6]. The highest efficiency of 12.3% was reported by Gratzel et al. and ever since then efforts to enhance DSSC efficiency have been attempted, with no success so far [7]. High efficiencies have been reported for perovskite-based solar cells; however, the cells show poor stability [8], limiting their commercialization. Hence, there is a need for stable materials for DSSCs with relatively higher efficiency. DSSCs are based on a dye that captures photons from the incident light promoting electrons from valence into a conduction band. The promoted electrons from the dye are then transferred into the conduction band of metal oxide-based semiconductor materials such as titanium oxide and zinc oxide [7,9,10]. The most common challenges with DSSCs are: (i) dye insufficient light absorption; (ii) high charge recombination rates

on both the metal oxide semiconductor and the dye; and lastly, the (iii) insufficient charge separation of the metal oxide semiconductor [5,11,12].

The most used metal oxide semiconductor for DSSCs is titanium oxide because it is stable and relatively cheap. However, it absorbs the ultraviolet light of the light spectrum and has a 3.2 eV wide band-gap leading to low photon to electron conversion efficiency [7]. To improve light absorption of the titanium oxide semiconductor in the visible region, metal nanostructures such as copper, silver, gold and aluminum have been used to improve light absorption across the solar spectrum [13–17]. Furthermore, the interest in metal nanostructures for DSSCs is based on trapping photons efficiently based on localized surface plasmon resonance (LSPR). This is a phenomenon of trapping electron cascades into three mechanisms that are crucial in DSSC, namely: (i) hot electron injection, (ii) incident light absorption/scattering and (iii) plasmon-induced resonance energy transfer [18,19]. These mechanisms increase the influx of excited electrons into the semiconductor materials that are affected by the size, shape and stabilizing agent of the metal nanoparticles [19,20]. The increase in DSSC efficiency has been reported with an increase in the size of plasmonic Ag and AuNPs, with increments of around 13% and 28%, respectively [21,22]. In this study, we used gold nanoparticles (AuNPs) with different sizes to make Au/TiO<sub>2</sub> nanocomposites for DSSCs. We then studied the effects of gold nanoparticles' physical properties such as size and shape on the efficiency of the DSSC. In this work, we show that increasing the size of the AuNPs improves the efficiency of the DSSC with increments that are higher than have been reported before [21,22].

## 2. Materials and Methods

Titanium oxide (P25), tri-sodium citrate, tetrachloroaurate, indium doped tin oxide (ITO) glass slides, iodine, lithium iodide, Eosin Y dye and tetraisopropoxide were all purchased from Sigma Aldrich, Johannesburg, South Africa. The physical properties of the samples were examined by TEM, JEOL operated at 200 kV. The X-ray diffractometer (Bruker D8 Discover, Billerica, MA, USA), equipped with a copper radiation source (1.5405 Å), was used to analyze the material crystalline phases. The optical properties were investigated using a Shimadzu<sup>®</sup> UV-2550 spectrophotometer (Kyoto, Japan). The performance of the DSSC was measured using a Metrohm potentiostat (PGSTAT302N, Herisau, Switzerland) coupled with an LED driver kit using warm white light.

### 2.1. Synthesis of Gold Nanoparticles (AuNPs) with Different Sizes

Spherical AuNPs were prepared following a Turkevich method [23] via an in-situ nucleation method by mixing citrate and gold salt with various concentrations. Masses of tri-sodium citrate of 192.10, 96.10 and 19.20 mg dissolved in water were added into a solution of tetrachloroaurate (mass of 75.83 mg dissolved in water) to achieve mass ratios of 0.7, 0.5 and 0.2 of citrate to tetrachloroaurate. The samples were heated to a boiling point while being stirred then cooled to an ambient temperature. The samples were characterized after isolation in the dark cupboard for 24 h. The resulting AuNPs have TEM sizes of 14, 30 and 40 nm, for mass ratios of 0.7, 0.5 and 0.2 of citrate to tetrachloroaurate, respectively, and will be represented as Au-14 nm, Au-30 nm and Au-40 nm throughout the manuscript.

### 2.2. Synthesis of Au/TiO<sub>2</sub> Nanocomposite

The Au/TiO<sub>2</sub> nanocomposites (2.5 wt.%) were prepared by freeze drying the AuNPs solutions to form AuNPs' nanopowders, that were then mixed with TiO<sub>2</sub> powder in ethanol, separately for each nanoparticle size. Each solution was ultrasonicated for 5 min and vigorously shaken using an electric shaker for 1 h at room temperature. The Au/TiO<sub>2</sub> nanocomposites were centrifuged at 4000 rpm to recover the Au/TiO<sub>2</sub> nanocomposites. Finally, the samples were dried in the oven at 80 °C for overnight.



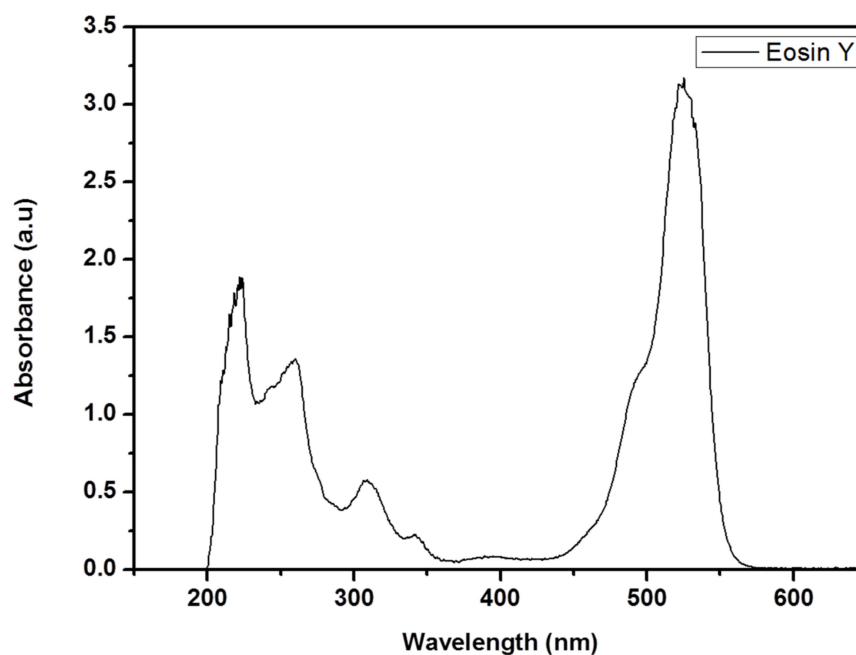


Figure 2. The ultraviolet-visible spectrum of Eosin Y dye suspended in dimethyl sulfoxide solvent.

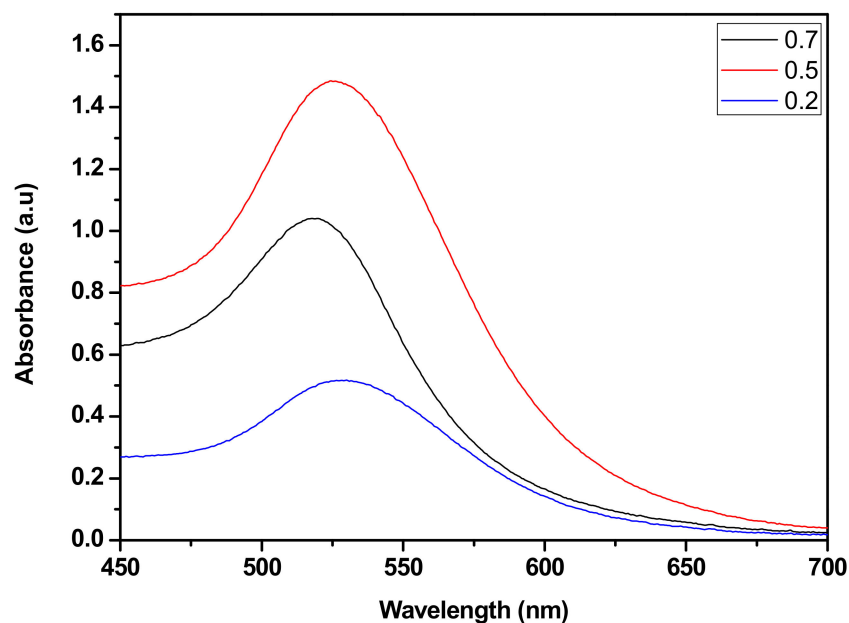
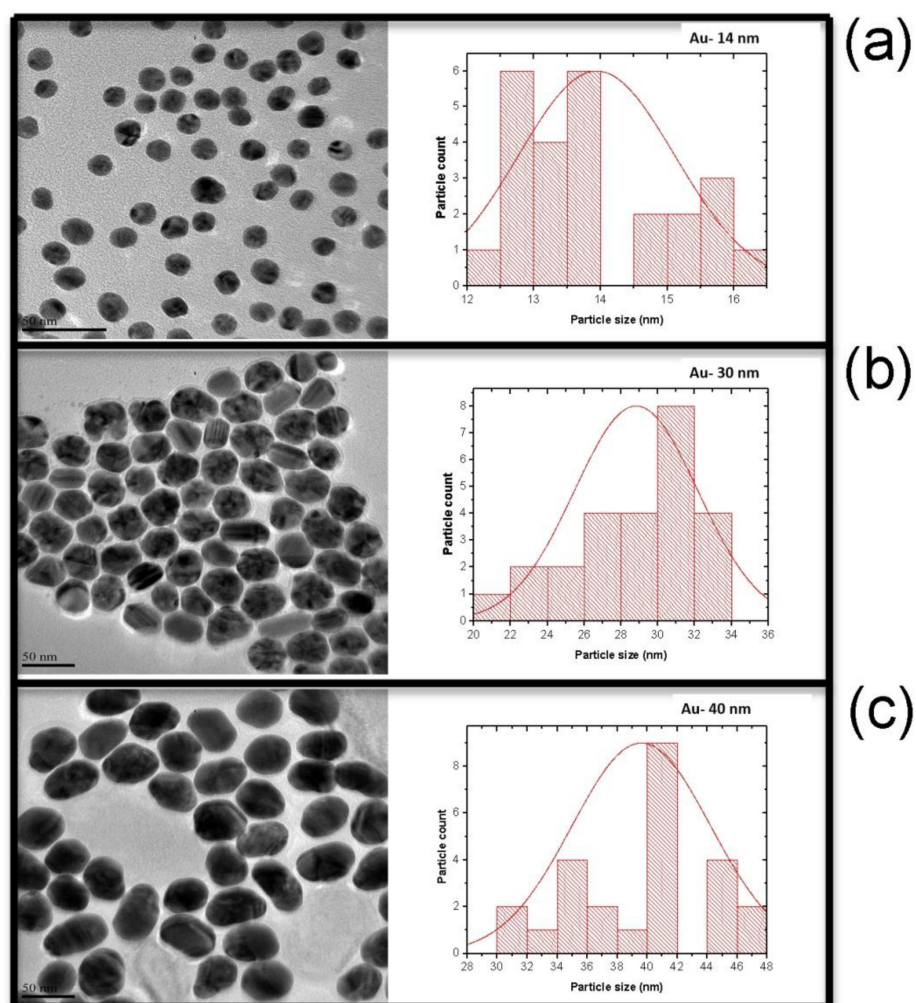


Figure 3. The UV-Vis spectra of the samples with various citrate/metal precursor ratios.

AuNPs were synthesized by the classic Turkevich method with varying citrate/gold salt ratios [26]. Figure 4 shows TEM images of the various samples (ratios: 0.7, 0.5 and 0.2) with their respective size distribution histograms. The TEM images revealed that the samples had particle sizes of 14 (0.7), 30 (0.5) and 40 nm (0.2). The TEM showed monodispersed AuNPs in line with the single peak observed from the UV-Vis spectrum. Interestingly, the shape of the AuNPs became increasingly irregular with a decrease in the citrate/gold salt ratio. A limited concentration of citrate molecules resulted in a formation of an oval shape and/or other irregular structures (Figure 4).

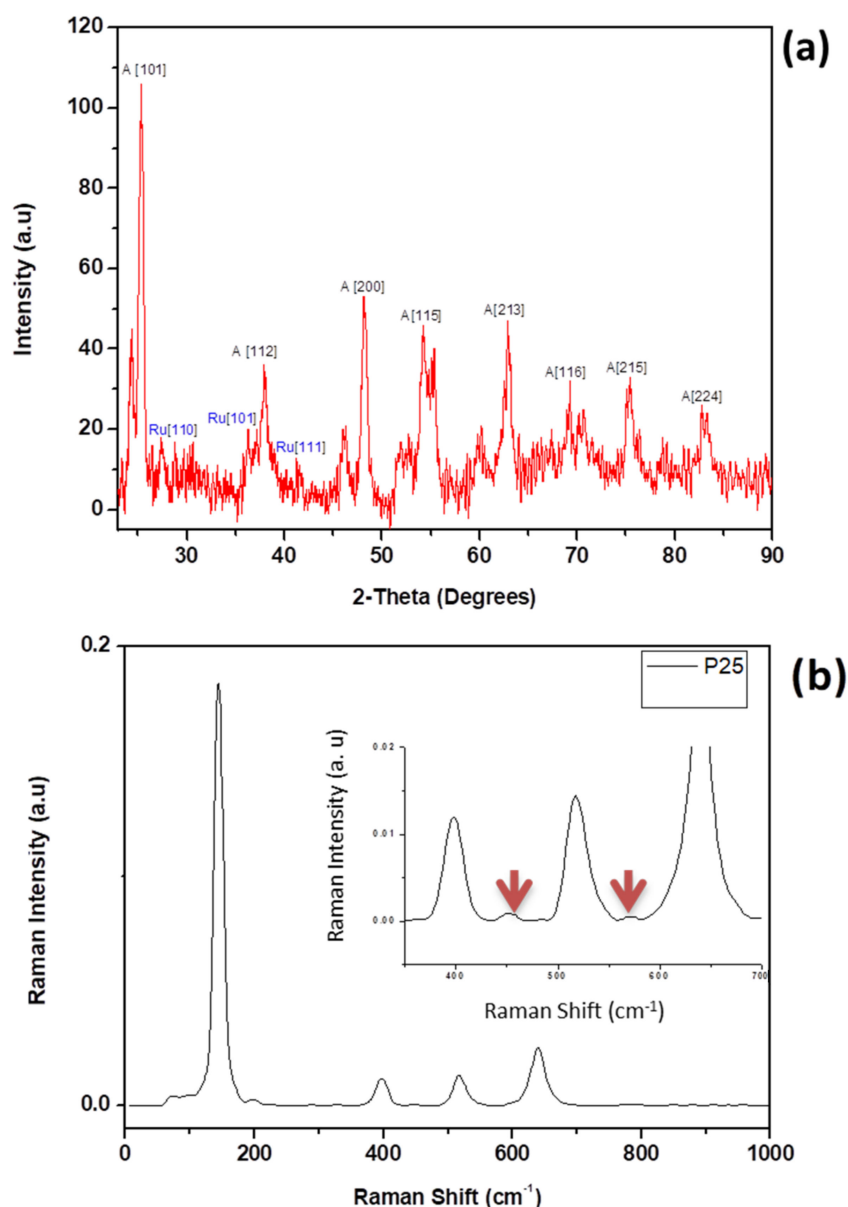


**Figure 4.** The transmission electron microscope images and size distribution histograms of AuNP samples synthesized with (a) 0.7, (b) 0.5 and (c) 0.2 citrate salt/gold salt ratio.

The results show that a 0.7 citrate ratio to gold salt led to the formation of small AuNPs (14 nm). As the citrate concentration was systematically reduced, the size of the nanoparticles increased to 30 nm and then to 40 nm. It is noteworthy that the reduction of citrate concentration implies an increase in gold ion concentration. An equilibrium of citrate ions and gold ions is important in determining the morphology of gold nanoparticles. The citrate moiety hinders the growth of gold crystal planes, which control the size of gold nanoparticles.

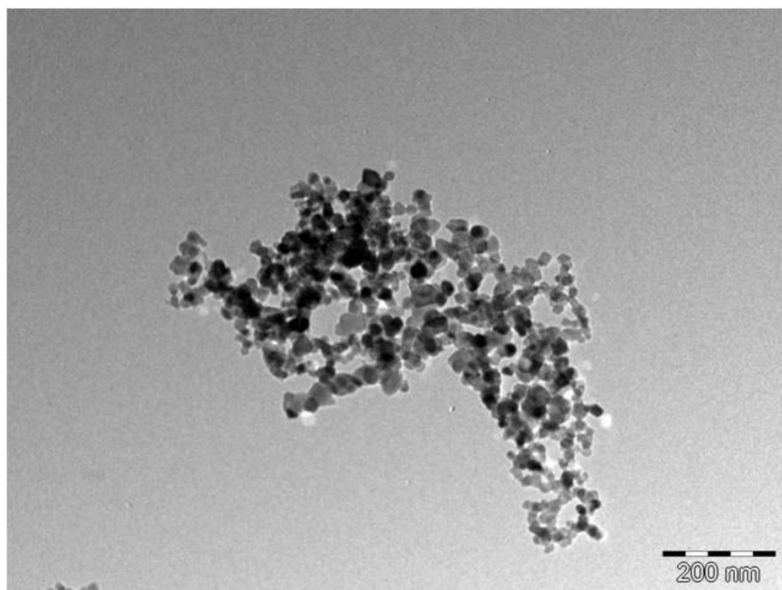
### 3.1. Physical and Structural Properties of $\text{TiO}_2$ Nanoparticles

Figure 5a shows the XRD pattern of commercial  $\text{TiO}_2$  (P25) nanopowder. The XRD pattern revealed narrow peaks implying a crystalline sample. Peaks at  $25^\circ$  {101},  $36^\circ$  {112},  $48^\circ$  {200},  $54^\circ$  {115},  $63^\circ$  {213},  $69^\circ$  {116},  $76^\circ$  {215} and  $84^\circ$  {224} 2-Theta values were all indexed to the anatase phase and the peaks at 2-Theta values of  $28^\circ$  {110} and  $36^\circ$  {101} were indexed to the rutile phase. These results show that the  $\text{TiO}_2$  powder was a blend of anatase and rutile phases (80%/20%) (JCPDS, Card No. 4-784). Figure 5b shows the Raman spectrum of the  $\text{TiO}_2$  nanoparticles. The Raman spectrum revealed typical anatase structure bands (Eg ( $142\text{ cm}^{-1}$ ), B1g ( $399\text{ cm}^{-1}$ ), A1g ( $520\text{ cm}^{-1}$ ) and Eg ( $641\text{ cm}^{-1}$ )) [27]. Figure 4b (insert) showed A1g ( $452\text{ cm}^{-1}$ ) and Eg ( $570\text{ cm}^{-1}$ ) bands which are characteristic of the rutile phase [27]. The XRD and Raman results show that the anatase phase was a predominant phase in the samples.



**Figure 5.** The (a) XRD and (b) Raman spectra of titanium oxide nanoparticles with the arrows showing the rutile phase.

The physical properties of TiO<sub>2</sub> were studied by TEM and the image is shown in Figure 6. A TEM analysis revealed that TiO<sub>2</sub> nanoparticles were in a spherical form, having a diameter of 20 nm (range of 16 to 28 nm). The observed relatively uniform TiO<sub>2</sub> nanoparticles are indicative of the monodispersive nature of the nanoparticles. The observed relatively narrow particle size distribution of TiO<sub>2</sub> suggests a very high surface area and enhanced adsorption binding sites for dye for the DSSC application. The TiO<sub>2</sub> nanoparticles appeared to have a monolithic structure and appeared to be stacked on top of each other, making other particles appear darker than the others.



**Figure 6.** TEM image of TiO<sub>2</sub> nanoparticles.

### 3.2. Physical and Structural Properties of Au/TiO<sub>2</sub> Nanocomposite

The structural properties of the Au/TiO<sub>2</sub> nanocomposite (from 0.7 ratio) were characterized using XRD in Figure 7. The XRD spectrum revealed peaks at 25° {101}, 36° {112}, 48° {200}, 54° {115}, 63° {213}, 69° {116}, 76° {215} and 84° {224} 2-Theta angles. The peaks were all indexed to the anatase phase of TiO<sub>2</sub>. The peaks at 2-Theta angles of 28° {110} and 36° {101} were all indexed to the rutile phase, similar to the pristine TiO<sub>2</sub> results (Figure 5). However, the peaks at 2-Theta angles of 38° {111} and 42° {200} were indexed to the gold nanoparticles, confirming the Au/TiO<sub>2</sub> nanocomposite formation. Furthermore, the Au/TiO<sub>2</sub> composite color changed to purple, similar to the color of gold nanoparticles in solution.

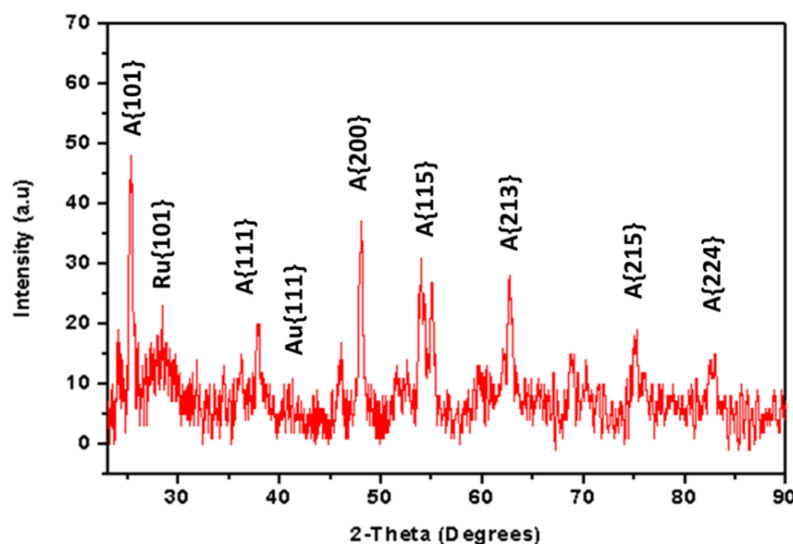


**Figure 7.** XRD pattern of Au/TiO<sub>2</sub> nanocomposite (0.7 ratio).

Figure 8 shows the TEM images of Au-TiO<sub>2</sub> nanocomposite samples incorporated with AuNP sizes of (a) 14, (b) 30 and (c) 40 nm with their respective (d) EDX spectrum. The AuNPs were identified by both their smaller size within the TiO<sub>2</sub> nanoparticle matrix and by the EDX spectrum. The EDX spectrum showed Au (2%), Ti (42%), O (20%) and C (36%) elements; the carbon element was from the TEM sample holder. The scattered electrons from the TEM were directly proportional to the atomic number of the element.

Au has a higher atomic number than titanium and oxygen; hence, it appeared brighter on the TEM image. This study revealed that it is a challenge to fully load the Au into the TiO<sub>2</sub> nanoparticle matrix, as it can be observed that some AuNPs were found outside of the TiO<sub>2</sub> nanoparticle matrix.

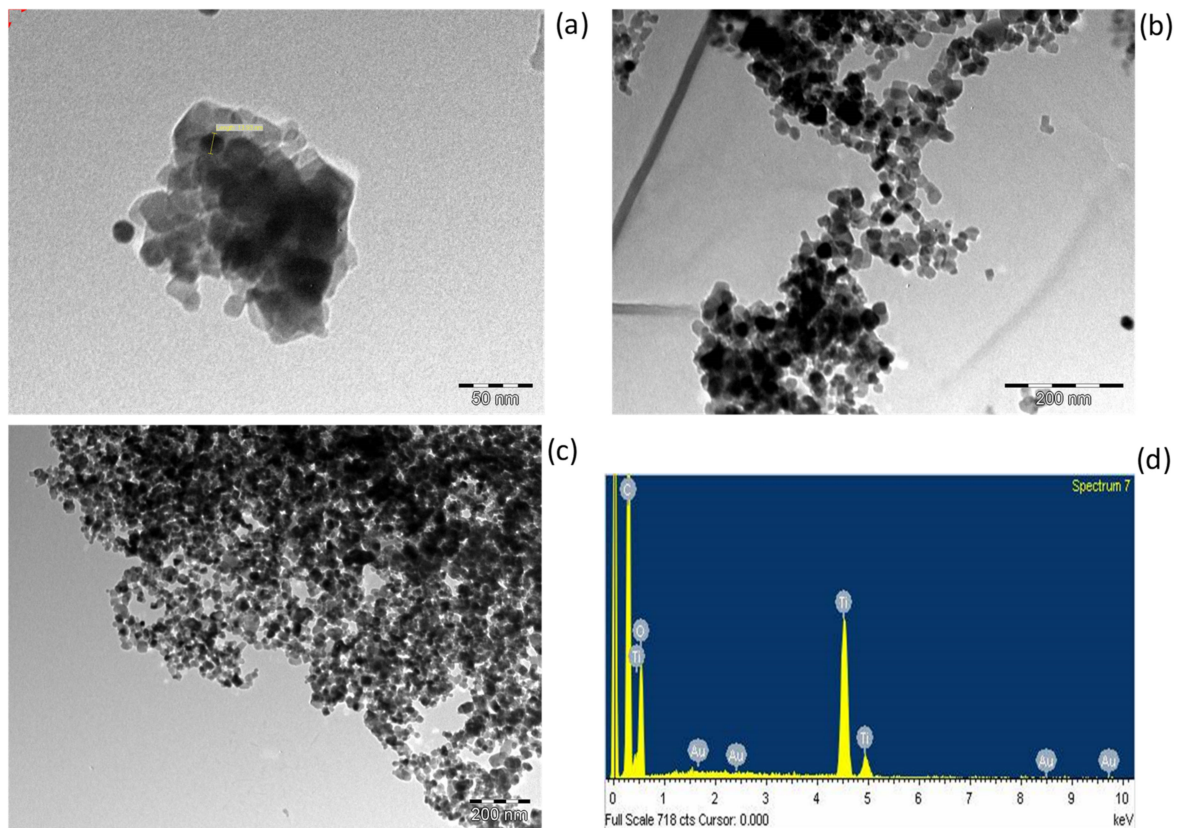


**Figure 8.** TEM image of Au/TiO<sub>2</sub> nanocomposite with gold nanoparticles' TEM sizes of (a) 14, (b) 30 and (c) 40 nanometers with their (d) EDX spectrum.

### 3.3. The Plasmonic Gold Nanoparticles Induced Effects on the Solar Conversion Efficiency

The efficiencies of TiO<sub>2</sub> and the Au/TiO<sub>2</sub> nanocomposites loaded with different sizes of AuNPs are shown in Figure 9. The results reveal that the addition of AuNPs with the size of 14 nm increased the efficiency by 8% (2.4 to 2.6%). Titanium oxide (Degussa-P25) absorbs the ultraviolet light leading to low photon-to-electron energy transition [26,28]. The increase in the efficiency was attributed to visible region light absorption (wavelength: 350 nm to 700 nm), in addition to absorption by Eosin Y dye, that was enhanced by the introduction of the plasmonic gold nanoparticles into the TiO<sub>2</sub> matrix. Furthermore, Figure 9 shows an increase in solar efficiency from 2.6 to 6.4% as a direct consequence of the gold nanoparticles' size from 14 to 40 nm.

This observed increase, when the size of the AuNPs increased, was attributed to three mechanisms: (i) hot electron injection, (ii) light scattering/absorption and (iii) plasmon-induced resonance energy transfer. The incorporation of metal nanoparticles such as gold into the TiO<sub>2</sub> semiconductor creates a metal-semiconductor hetero-junction limiting energy transfer due to the Schottky barriers emanating from the difference in Au-TiO<sub>2</sub> work functions [29,30]. However, the metal nanoparticles can scatter the incident light to penetrate the semiconductor, leading to an influx of photons into the semiconductor. Furthermore, light scattered by the AuNPs promotes light absorption and charge separation in the TiO<sub>2</sub>, leading to better electron diffusion. The light scattering/absorption mechanism

was affected by the size, shape and dielectric properties the solvent used for dispersion. Light scattered by the AuNPs can be quantified by Equation (1) [31].

$$C_{\text{sca}} = \frac{8}{3}\pi k^4 r^6 \left| \frac{\varepsilon - \varepsilon_m}{\varepsilon + 2\varepsilon_m} \right|^2 \quad (1)$$

where  $k = 2\pi/\lambda$ ,  $\lambda$  is the light wavelength,  $r$  is the radius of gold nanoparticles,  $\varepsilon$  is the permittivity for the nanoparticles and  $\varepsilon_m$  is the permittivity for the surrounding medium. According to Equation (1), it is clearly demonstrated that scattered light largely depended on the radius of the gold nanoparticles, because all the AuNPs were synthesized in water with the same dielectric properties. This partly explains the high efficiency shown by DSSC with 40 nm gold nanoparticles.

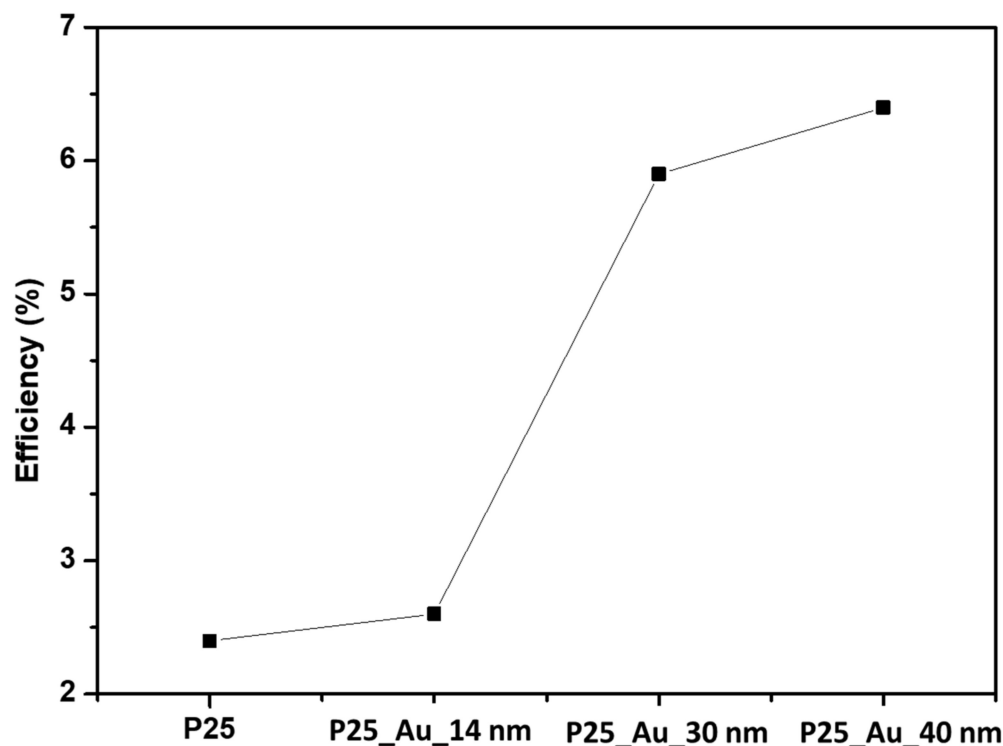


Figure 9. Solar cell efficiency curve comparison of TiO<sub>2</sub> and different sizes of gold nanoparticles.

Due to differences in the work functions of gold and TiO<sub>2</sub>, electrons cannot freely pass through the Schottky energy barrier in the Au-TiO<sub>2</sub> hetero-junction. However, after the gold nanoparticles' absorption and scatter of light, this creates "hot electrons" within the gold nanoparticle achieved by thermal excitation. These electrons possess sufficient energy to subdue the Schottky energy barrier of the Au-TiO<sub>2</sub> interface, resulting in them being injected directly into the conduction band of TiO<sub>2</sub> [29]. This increases the electron influx of the TiO<sub>2</sub> conduction band. The TiO<sub>2</sub> conduction band does not only receive electrons from the Eosin Y dye, but it receives additional electrons from the AuNPs. Since the absorption and scattering of light is favored by larger nanostructures, this explains the high efficiency of DSSC loaded with 40 nm AuNPs compared 14 nm. Furthermore, the "hot electron injection" mechanism is affected by the proximity between the metal nanostructures and metal oxide semiconductor, affected by the stabilizing agent. The gold nanoparticles were all stabilized with citrate moiety, which was used to control the gold nanoparticles' size. Nonetheless, the presence of the stabilizer on the surface of the gold nanoparticle could have adverse effects by limiting the accessibility of the gold surface plasmons [22]. The concentration of citrate was systematically reduced to synthesize bigger nanoparticles. This means that gold nanoparticles with 40 nm had less citrate moiety on their surface compared to 14 nm. This shows that gold nanoparticles with the size of 40 nm were in

closer proximity to TiO<sub>2</sub> nanoparticles compared to 14 nm AuNPs. Since the hot electron injection mechanism was affected by the distance between the metal and semiconductor, it is clear that more electron influx to the TiO<sub>2</sub> conduction band was experienced for 40 nm gold nanoparticles.

Lastly, the plasmon-induced resonance energy transfer (PIRET) affects the formation of the dipole–dipole interaction formed by the excitation of the AuNPs [29]. The light-induced gold nanoparticles' dipole–dipole pairs generate electron pairs in the semiconductor which reduces charge recombination in the TiO<sub>2</sub> [28,29]. The PIRET mechanism is also affected by the metal–semiconductor proximity (contact angle) which is favored by the bigger AuNPs (40 nm).

The solar cell efficiency was calculated according to Equation (2).

$$\eta = \frac{ff \text{ Voc Jsc}}{P_{\text{solar}}} \quad (2)$$

where Jsc, Voc, FF and  $\eta$  stand for current density, open current voltage, fill factor and solar efficiency, respectively. Results show that the current density and efficiency increased with the size of the gold nanostructures. The relatively high short circuit voltage (Jsc) was due to the optimization done to the DSSC, which was achieved by (i) enhancing the exposure area of the cell (ii) using a high energy light source with an appropriate incident light wavelength. The high currently density shown by the DSSC with 40 nm gold nanoparticles was in agreement with the high influx of electrons to the conduction band of TiO<sub>2</sub>, suggested by light scattering, hot electron injection and PIRET mechanisms. Table 1 show the other photovoltaic parameters of the TiO<sub>2</sub> semiconductor and the different nanocomposites.

**Table 1.** Photovoltaic Parameters of DSSC based on Various Samples.

Sample Name	Jsc (mA cm <sup>-2</sup> )	Voc (V)	FF	$\eta$ (%)
P25	1.75	0.23	0.29	2.41
TiO <sub>2</sub> -P25//Au-14 nm	4.36	0.24	0.30	2.60
TiO <sub>2</sub> -P25//Au-30 nm	26	0.29	0.30	5.91
TiO <sub>2</sub> -P25//Au-40 nm	45	0.08	0.23	6.43

#### 4. Conclusions

The gold nanoparticles' size was controlled by the citrate concentration. Increasing the concentration of the citrate resulted in the formation of smaller AuNPs. Larger gold nanoparticles exhibited higher DSSC efficiency compared to smaller ones. The high efficiency emanating from larger AuNPs was due to light absorption/scattering, hot electron injection and a plasmon-induced resonance energy transfer mechanism. The relatively larger particles absorb and scatter light better than smaller particles, leading to a higher electron influx into the TiO<sub>2</sub>, which leads to higher DSSC efficiency. Larger gold nanoparticles showed a higher current density compared to smaller gold nanoparticles due to a high electron influx to the TiO<sub>2</sub> caused by larger AuNPs.

**Author Contributions:** S.N.: conceptualization, methodology, validation, formal analysis, investigation, data curation, writing—original draft preparation; F.C.: methodology and validation; A.M.: formal analysis and investigation; T.N.: conceptualization, methodology, validation, formal analysis, investigation, data curation, writing—original draft preparation, funding acquisition, supervision, project administration; G.N.: methodology, validation, data curation L.S.: conceptualization, methodology, validation, formal analysis, investigation, data curation, writing—original draft preparation, funding acquisition, supervision, project administration. All authors have read and agreed to the published version of the manuscript.

**Funding:** This research was funded by the Department of Science and Innovation, South Africa, under the Nanotechnology Innovation Centre program and Rhodes University facility support (Research Facility: UID 62620).

**Institutional Review Board Statement:** Not applicable.

**Informed Consent Statement:** Not applicable.

**Data Availability Statement:** The data presented in this study are available on request from the corresponding author.

**Acknowledgments:** This work was supported by the Department of Science and Innovation (DSI), South Africa, through the DSI/Mintek, Nanotechnology Innovation Centre (NIC). The authors wish to acknowledge NIPMO (The National Intellectual Property Management Office—South Africa) and Centre for High Performance Computing (HPC) for the support.

**Conflicts of Interest:** The authors declare no conflict of interest.

## References

1. Tsoskounoglou, M.; Ayerides, G.; Tritopoulou, E. The end of cheap oil: Current status and prospects. *Energy Policy* **2008**, *36*, 3797–3806. [CrossRef]
2. Energy Information Association International Energy Outlook 2010. Available online: <http://www.eia.doe.gov/> (accessed on 15 January 2022).
3. Heinberg, R.; Fridley, D. The end of cheap coal. *Nature* **2010**, *468*, 367–369. [CrossRef] [PubMed]
4. Pearce, J.; Lau, A. Net Energy Analysis for Sustainable Energy Production from Silicon Based Solar Cells. In Proceedings of the ASME Solar 2002: International Solar Energy Conference, Reno, NV, USA, 15–20 June 2002; pp. 181–186.
5. Lim, S.P.; Pandikumar, A.; Huang, N.; Lim, H.R. Facile synthesis of Au@TiO<sub>2</sub> nanocomposite and its application as a photoanode in dye-sensitized solar cells. *Soc. Chem.* **2015**, *5*, 44398–44399. [CrossRef]
6. Chen, X.; Mao, S.S. Titanium dioxide nanomaterials: Synthesis, properties, modifications and applications. *Chem. Rev.* **2007**, *107*, 2891–2959. [CrossRef] [PubMed]
7. O'Regan, B.; Gratzel, M. A low-cost, high-efficiently solar cell based on dye-sensitized colloidal TiO<sub>2</sub> films. *Nature* **1991**, *353*, 445–449.
8. Wang, R.; Mujahid, M.; Duan, Y.; Wang, Z.-K.; Xue, J.; Yang, Y. A Review of Perovskites Solar Cell Stability. *Adv. Funct. Mater.* **2019**, *29*, 1808843. [CrossRef]
9. Giordano, F.; Abate, A.; Correa Baena, J.P. Enhanced electronic properties in mesoporous TiO<sub>2</sub> via lithium doping for high-efficiency perovskite solar cells. *Nat. Commun.* **2016**, *7*, 10379–10380. [CrossRef] [PubMed]
10. Burschka, N.J.; Pellet, S.; Moon, S.-J. Sequential deposition as a route to high-performance perovskite-sensitized solar cells. *J. Nature* **2013**, *499*, 316–319. [CrossRef] [PubMed]
11. Kopydakis, N.; Neale, N.R.; Zhu, K.; van de Lagemaat, J.; Frank, A.J. Spatial location of transport-limiting traps in TiO<sub>2</sub> nanoparticles films in dye-sensitized solar cells. *Appl. Phys. Lett.* **2005**, *87*, 202106–202110. [CrossRef]
12. Van de Lagemaat, J.; Park, N.G.; Frank, A. Influence of electrical potential distribution, charge transport and recombination on the photopotential and photocurrent conversion efficiency of dye-sensitized nanocrystalline TiO<sub>2</sub> solar cells: A study by electrical impedance and optical modulation techniques. *J. Phys. Chem. B* **2000**, *104*, 2044–2052.
13. Jun, H.K.; Careem, M.A.; Arof, A.K. Plasmonic effects of quantum size gold nanoparticles on dye-sensitized solar cell. In Proceedings of the 5th International Conference on Functional Materials & Devices (ICFMD), London, UK, 4–6 August 2015; pp. 73–79.
14. Häggglund, C.; Zäch, M.; Kasemo, B. Electromagnetic coupling of light into a silicon solar cell by nanodisk plasmons. *Appl. Phys. Lett.* **2008**, *92*, 013113–013118. [CrossRef]
15. Schaadt, D.M.; Feng, B.; Yu, E.T. Enhanced semiconductor optical absorption via surface plasmon excitation in metal nanoparticles. *Appl. Phys. Lett.* **2005**, *86*, 063106–063108. [CrossRef]
16. De Sousa, S.; Lyu, S.; Ducasse, L.; Toupance, T.; Olivier, C. Tuning visible-light absorption properties of Ru–diacetylide complexes: Simple access to colorful efficient dyes for DSSCs. *J. Mater. Chem. A* **2015**, *3*, 18256–18264. [CrossRef]
17. Akila, Y.; Muthukumarasamy, N.; Velauthapillai, D. TiO<sub>2</sub>-based dye-sensitized solar cells. In *Nanomaterials for Solar Cell Applications*; Thomas, S., Kalarikkal, N., Wu, J., Oluwafemi, S.O., Sakho, E.H.M., Eds.; Elsevier: Amsterdam, The Netherlands, 2019; pp. 127–144.
18. Furube, A.; Du, L.; Hara, K.; Katoh, R.; Tachiya, M. Ultrafast plasmon induced electron transfer from gold nanodots into TiO<sub>2</sub> nanoparticles. *J. Am. Chem. Soc.* **2007**, *129*, 14852–14853. [CrossRef] [PubMed]
19. Cushing, S.K.; Li, J.; Bright, J.; Yost, B.T.; Zheng, P.; Bristow, A.; Wu, N. Controlling plasmon-induced resonance energy transfer and hot electron injection processes in metal@TiO<sub>2</sub> core-shell nanoparticle. *J. Phys. Chem.* **2015**, *119*, 16239–16244. [CrossRef]
20. Brongersma, M.L.; Halas, N.J.; Nordlander, P. Plasmon-induced hot carrier science and technology. *Nat. Nanotechnol.* **2015**, *10*, 25–34. [CrossRef] [PubMed]

21. Wang, Q.; Butburee, T.; Wu, X.; Chen, H.; Liu, G.; Wang, L. Enhanced performance of dye-sensitized solar cells by doping Au nanoparticles into photoanodes: A size effect study. *J. Mater. Chem. A* **2013**, *1*, 13524–13531. [[CrossRef](#)]
22. Saravanan, S.; Kato, R.; Balamurugan, M.; Kaushik, S.; Soga, T. Efficiency improvement in dye sensitized solar cells by the plasmonic effect of green synthesized silver nanoparticles. *J. Sci. Adv. Mater. Devices* **2017**, *2*, 418–424. [[CrossRef](#)]
23. Turkevich, J.; Stevenson, P.C.; Hillier, J. A study of the nucleation and growth processes in the synthesis of colloidal gold. *Discuss. Faraday Soc.* **1951**, *11*, 55–75. [[CrossRef](#)]
24. Chander, N.; Komarala, V.K. Fabrication and characterisation of dye sensitized solar cells: A photographic guid. *Indian J. Pure Appl. Phys.* **2017**, *55*, 737–744.
25. Nyembe, S.; Mpelane, S.; Shumbula, P.; Harris, R.; Moloto, N.; Sikhwihilu, L. Plasmonic gold nanocrystals: Formation of icosahedron and decahedron nanostructures through twinning mechanism. *J. Nanosci. Nanotechnol.* **2016**, *16*, 9832–9837. [[CrossRef](#)]
26. Ding, W.; Zhang, P.; Li, Y.; Wang, D.; Tao, X. Nanomaterials with enzyme-like characteristics. *J. Phys. Chem.* **2015**, *16*, 447–450.
27. Kernazhitsky, L.; Shymanovska, V.; Gavrilko, T. Laser-excited excitonic luminescence of nanocrystalline TiO<sub>2</sub> powder. *Ukr. J. Phys.* **2014**, *59*, 246–253. [[CrossRef](#)]
28. Kumar, S.G.; Devi, L.G. Review on modified TiO<sub>2</sub> photocatalysis under UV/visible light: Selected results and related mechanisms on interfacial charge carrier transfer dynamics. *J. Phys. Chem. A* **2011**, *115*, 13211–13241. [[CrossRef](#)] [[PubMed](#)]
29. Wu, N. Plasmonic metal-semiconductor photocatalyst and photoelectrochemical cells: A review. *Nanoscale* **2018**, *10*, 2679–2696. [[CrossRef](#)] [[PubMed](#)]
30. Tatsuma, T.; Nishi, H.; Ishida, I. Plasmonic-induced charge separation: Chemistry and wide applications. *Chem. Sci.* **2017**, *8*, 3325–3337. [[CrossRef](#)] [[PubMed](#)]
31. Maier, S. A Plasmonic: Fundamentals and applications. *Appl. Springer Sci. Bus. Media* **2007**, *1*, 254–259.